KRONOS FUSION ENERGY

PAPER 2.48 · THE KRONOS 2026 SERIES

A Tantalum- and Rhenium-Free Low-Activation Alloy Family for First Wall, Divertor and Direct-Energy-Converter Electrodes: A First-Principles Composition-of-Matter Study

The plasma-facing components of a compact, high-power-density fusion machine must combine refractory strength with low activation: the alloy that survives the heat and the MeV...

Read it live — 3-D model · physics validator · film series

BY P I FORD AND G L KULCINSKI

2026 · EDITORIAL EDITION

THE OFFICIAL RECORD

What this document is, and how to read its numbers

This is a combined editorial. It gathers, in one volume, the two design studies Kronos Fusion Energy released in 2026 — a compact spherical-tokamak tritium/helium-3 breeder and a deuterium–helium-3 tandem-mirror generator — together with the intellectual-property estate, the people, and, in the internal edition, the full commercial case. The scientific text is the same text that appears in the arXiv preprints and the journal submissions; the editorial adds the apparatus a reader needs to hold the whole program at once, and nothing in the physics is altered to fit it.

THE HONESTY STANCE IS THE ASSET

Every headline quantity carries an **evidence class** — DERIVED RECOMPUTED MEASURED REQUIREMENT — and, where a number is a modelled extrapolation rather than a demonstrated value, it is labelled as such and its downside is shown next to it. Several quantities in the underlying corpus moved after first publication; where a value has been withdrawn or restated, the record says so plainly. This is deliberate: a diligence team will find the load-bearing assumptions, so the document surfaces them first.

TWO EDITIONS

This volume is issued in two editions. The **public edition** (light) carries the physics and the design only — no dollar, price, or per-kilogram figure appears anywhere in it. The **internal edition** (dark) adds the economics, the funding architecture, and the defense-commercial analysis, and is marked *Confidential* accordingly; it is not for public distribution. Where the commercial case rests on a modelled assumption rather than a demonstrated one, it is labelled as such and its downside is shown alongside it, on the same terms as the physics.

TITLE	The Kronos Fleet — Hyperion · Aegis · MetroVolt: A Combined Design & Commercialization Study
AUTHOR	Priyanca Ford, Founder & CEO, on behalf of Kronos Fusion Energy
EDITION	2026 Combined Editorial · first issue
COMPANION WORKS	The five-paper arXiv drop — (1) Breeder, (2) Burner, (3) REBCO magnet & tape, (4) Direct Energy Conversion, (5) AI/ML/Quantum control — with matching numbered Zenodo deposits, plus the IOP journal and IAEA-FEC submissions. Patents were filed before the drop.
NAMING	Hyperion = the breeder; Aegis (defense) and MetroVolt (data-center) = one generator in two housings. Internal mode letters (D1, L) do not appear on public surfaces.
STATUS	Conceptual design & simulation study. Nothing herein is a construction commitment.

HOW TO READ THIS VOLUME

The fleet at a glance, and the way its numbers are marked

This volume opens with *Orientation*, presents the five research papers as a bound sequence, and closes with the *Apparatus*. *Foundations* sets out the three general results both machines rest on. *Paper One* is the Hyperion breeder; *Paper Two* the Aegis / MetroVolt generator; *Papers Three, Four and Five* are the enabling science — high-field REBCO magnets and tape, direct energy conversion, and the AI / ML / quantum control stack. A *Digital Twin & 3-D Model* part follows, then the *Environmental* profile. The *Economics* and levelized cost and the *Business Case* and diligence record appear in the internal edition only; the *Simulations* proof record and the Apparatus — patent portfolio, team, limitations, and sources — close both editions.

THE FLEET AT A GLANCE

	HYPERION	AEGIS	METROVOLT
Role	Strategic-isotope foundry	Defense installation power	Campus power
Machine	**Spherical tokamak**	**Tandem mirror**	**Tandem mirror**
Fuel	Deuterium–tritium	Deuterium–helium-3	Deuterium–helium-3
Delivers	Tritium · ^{3}He · 14 MeV n	Resilient installation power	Firm campus power
Physics bar	**Fusion gain only**	Closure (gates named)	Closure + lunar ^{3}He
In the fleet	Breeds the fuel	Proves the generator	Commercial destination

HOW THE NUMBERS ARE MARKED

Every headline quantity carries an evidence class — DERIVED from first principles, RECOMPUTED from raw data, MEASURED in hardware, or a REQUIREMENT yet to be met. Financial figures carry a case label and are confined to the internal (confidential) edition. Values that moved after first publication are shown as withdrawn or restated rather than quietly changed. A capability you can evaluate is one whose limits are on the page.

ABSTRACT

A Tantalum- and Rhenium-Free Low-Activation Alloy Family for First Wall, Divertor and Direct-Energy-Converter Electrodes: A First-Principles Composition-of-Matter Study

The plasma-facing components of a compact, high-power-density fusion machine must combine refractory strength with *low activation*: the alloy that survives the heat and the 14 MeV neutrons must not become a long-lived waste problem after shutdown. These two goals normally pull against one another, because the strongest refractory solid solutions are built on tantalum and rhenium, and tantalum activates into the long-lived γ-emitter ^{182}Ta. We resolve the tension by first principles. We formulate the plasma-facing materials problem as a *composition-of-matter* optimisation over a deliberately tantalum-, rhenium-, copper- and molybdenum-free refractory system, Cr–Ti–V–W, and we solve it with spin-polarised plane-wave density-functional theory (DFT) on 16-atom body-centred-cubic special quasirandom structures under full variable-cell relaxation, run as a GPU-accelerated campaign on the NVIDIA GPU high-performance-computing (HPC) platform. The result is a family of three duty-matched alloys: a tungsten-rich *divertor* alloy $Cr_2Ti_4V_4W_6$ and a ductile, titanium-rich *first-wall* alloy $Cr_1Ti_7V_4W_4$, both near-neutral at a formation energy $E_f = -0.002$ eV/atom, and a tungsten-heaviest *direct-energy-converter (DEC) electrode* alloy $Cr_2Ti_5V_1W_8$ that is mildly stable at $E_f = -0.015$ eV/atom. Every member sits at or below the elemental-mixture line and *at or below* its tantalum-bearing analogue (a Ta-divertor alloy at $+0.015$ eV/atom and a Ta-first-wall alloy at $+0.007$ eV/atom, computed by the identical method), which establishes the central composition-of-matter result: *removing tantalum costs no phase stability*. We show quantitatively why: in a four-element refractory solid solution the configurational entropy contributes a stabilising $-T\Delta S_{\text{mix}} \approx -0.10$ to -0.13 eV/atom at 800–1000 K, an order of magnitude larger than the few-meV formation enthalpy, so the near-zero enthalpy is the expected signature of an entropy-stabilised refractory high-entropy alloy rather than a warning. The chromium elemental reference (-248.219 Ry/atom) reproduces an independent determination to 10^{-3} Ry, anchoring the most delicate leg of a common reference set. The family gives the Kronos machine set a single, self-consistent, Ta- and Re-free alloy design language spanning the breeder first wall and divertor and the burner's direct-energy-converter electrodes.

Open-access deposit (code & data, CC BY 4.0): DOI 10.5281/zenodo.22645891 · Zenodo community *kronos_fusion_energy*. Explore it live: interactive 3-D model · physics validator.

Keywords: low-activation alloy · plasma-facing component · high-entropy alloy · density-functional theory · formation energy · tantalum-free · rhenium-free · refractory · spherical-tokamak breeder

CONTENTS

Table of Contents

NOMENCLATURE

Symbols, units, and the names of things

Q	plasma (fusion) gain, P_{fus}/P_{aux}
Q_E	engineering gain, net electric out / recirculating in
H_{98}	confinement enhancement over the IPB98(y,2) scaling
Z_{eff}	effective ion charge
c_{ee}	electron–electron bremsstrahlung leading coefficient, 2.120022 (exact)
τ_E	energy confinement time
I_p	plasma current
R_0, a	major radius, minor radius
κ, δ	elongation, triangularity
β_N	normalized plasma beta (Troyon-normalized)
TBR	tritium breeding ratio
DEC	direct energy conversion
CF	plant capacity factor (availability)
FOAK / NOAK / BOAK	first / nth / best of a kind
Hyperion	the ST breeder (internal: Mode D2)
Aegis	the generator, defense/installation housing (internal: Mode M)
MetroVolt	the generator, data-center housing (Mode M)

§ 1

Introduction

THE PLASMA-FACING MATERIALS PROBLEM

A plasma-facing component (PFC) in a compact, high-power-density fusion machine occupies the least forgiving materials environment in the plant. It must carry a large surface heat load, absorb a 14 MeV neutron fluence, tolerate sputtering and redeposition at its surface, and hold its structural function through years of duty. The Kronos Hyperion breeder produces $P_{\text{fus}} = 85.04$ MW at a fusion gain $Q = 3.076$ behind a negative-triangularity ($\delta = -0.30$) core at major radius $R_0 = 1.20$ m, aspect ratio $A = 2.5$, elongation $\kappa = 2.0$, on-axis field $B_0 = 8$ T and plasma current $I_p = 9.66$ MA, with its centrepost magnet reaching a peak field of 16.84 T [1,2]; its first wall and divertor see that environment directly. The companion D–^{3}He tandem-mirror burner adds a third plasma-facing duty of its own: the electrode surfaces of the direct-energy converter (DEC) that recovers charged- particle power at an efficiency $\eta_{\text{DEC}} = 0.49$ behind a 26.49 T superconducting plug — a magnet that is physically and functionally distinct from the breeder centrepost. Across the machine set, then, three plasma-facing stations demand a refractory material.

THE TANTALUM–RHENIUM ACTIVATION PENALTY

Two requirements pull against each other. Refractory strength, high-temperature phase stability and sputtering resistance are most easily bought with tungsten-, tantalum- and rhenium-bearing alloys. But tantalum and rhenium carry a neutron-activation penalty. Under a fusion spectrum, ^{181}Ta captures a neutron to ^{182}Ta, a γ-emitter with a 114.7-day half-life whose decay chain dominates contact dose and disposal accounting long after shutdown; rhenium transmutes readily into osmium and long-lived activation products. A materials set that keeps refractory performance while eliminating both elements is therefore worth a genuine design effort, because the low-activation choice governs waste-class routing, hands-on maintenance windows and the whole decommissioning case [31,30]. Figure 9 sketches the effect the family is designed to avoid.

HIGH-ENTROPY ALLOYS AS A DESIGN LANGUAGE

Multi-principal-element, or *high-entropy*, alloys (HEAs) provide the design language for this problem [3,4]. A concentrated solid solution of four or more elements in near-equal proportions draws a large configurational entropy of mixing, which lowers the free energy of the disordered single phase relative to ordered or phase-separated competitors [7,8,9]. Refractory HEAs built on the group-IV/V/VI transition metals reach very high melting points and retain strength to elevated temperature [5,6], and body-centred-cubic (BCC) refractory HEAs have shown outstanding radiation tolerance — a nanocrystalline W–Ta–Cr–V alloy retained its microstructure to high dose [13]. The essential consequence for the present work is thermodynamic: in a concentrated solid solution a *near-zero formation enthalpy is the target signature*, because the entropy term, not the enthalpy, is what stabilises the phase at operating temperature [10,11,12].

PRIOR ART AND THE GAP

First-principles screening of refractory alloys is now routine: DFT total energies on special quasirandom structures (SQS) [14,15] give formation energies to meV accuracy, and machine-learned interatomic potentials (MLIPs) trained on DFT [24,25] now pre-screen composition space at a fraction of the cost before DFT confirmation [26,27]. What has been missing for a compact fusion machine is a *single, internally consistent, tantalum- and rhenium-free* alloy set that (i) is computed at one reproducible level of theory so its members are directly comparable, (ii) is *duty-matched* — a distinct composition tuned to each of the first wall, divertor and DEC-electrode stations rather than one alloy stretched across all three, and (iii) is benchmarked against its own Ta-bearing analogues so that the cost of removing tantalum can be read off quantitatively rather than assumed.

CONTRIBUTION

This paper reports exactly that set and answers the design question it was built to answer. We (a) formalise the plasma-facing materials problem as a composition-of-matter optimisation with an explicit thermodynamic-viability criterion (§3); (b) solve it with spin-polarised plane-wave DFT on 16-atom BCC SQS cells under full variable-cell relaxation, run as a GPU-accelerated campaign whose codes, problem scale and reproducibility we state in full (§4); (c) report three duty-matched Ta- and Re-free alloys, all near-neutral or stable, and show member-by-member that each sits at or below its Ta-bearing analogue (§5); (d) demonstrate quantitatively that configurational entropy dominates the residual enthalpy, so the near-zero formation energies are the expected entropy-stabilised-HEA signature (§5, §6); and (e) place the family against the published HEA-thermodynamics and low-activation-materials literature (§6). Every quantitative claim traces to a frozen entry in the Kronos Physics De-Risking Register [33]; the roster serials (BR-L2-A37a/b/c, family record BR-L2-A37, and the Ta-bearing analogues BR-L2-A31/A32) are given inline so that each number is auditable.

§ 2

The plasma-facing duty environment and the low-activation constraint

The three stations impose distinct mechanical and thermal demands, and the family assigns a distinct composition to each (figure 1). The *divertor* takes the highest steady heat flux and the most severe sputtering, so its alloy is tungsten-rich for refractoriness and erosion resistance. The *first wall* covers a large area and must tolerate off-normal mechanical and thermal transients; toughness and ductility matter more there than peak melting point, so its alloy is titanium-rich and deliberately more ductile, trading some refractoriness for fracture tolerance. The *DEC electrode* sees intense charged-particle power on electrode surfaces held at high bias; its alloy is the tungsten-heaviest of the three. All three are drawn from a single Cr–Ti–V–W chemistry whose four constituents are each acceptable on activation grounds and which contains no Ta, Re, Cu or Mo.

We state the low-activation constraint as a hard exclusion set. Let $\mathcal{E}$ be the set of admissible elements. Then

$$\mathcal{E} \subseteq \{\mathrm{Cr}, \mathrm{Ti}, \mathrm{V}, \mathrm{W}\}, \qquad \{\mathrm{Ta}, \mathrm{Re}, \mathrm{Cu}, \mathrm{Mo}\} \cap \mathcal{E} = \varnothing,$$

where the exclusion of Ta and Re removes the dominant long-lived γ pathways of §1.2, and the exclusion of Cu and Mo removes two further activation and disposal liabilities. Equation (1) is a constraint on the *design*, not an outcome of the DFT; the question the DFT answers is whether a thermodynamically viable refractory solid solution exists inside that constrained composition space, and at what formation-energy cost relative to the Ta-bearing chemistry it replaces.

§ 3

Governing equations and the formal composition-of-matter problem

TOTAL ENERGY AND THE KOHN–SHAM PROBLEM

The ground-state total energy of each candidate alloy is obtained from Kohn–Sham DFT. For a cell of N atoms with nuclei at $\{R_I\}$ and electron density $n(r) = \sum_i f_i |\psi_i(r)|^2$, the Kohn–Sham orbitals solve

$$\left[-\tfrac{1}{2}\nabla^2 + v_{\mathrm{ext}}(r) + v_{\mathrm{H}}[n](r) + v_{\mathrm{xc}}[n](r)\right]\psi_i(r) = \varepsilon_i\,\psi_i(r),$$

with the Hartree potential $v_{\mathrm{H}}[n](r) = \int n(r')/|r - r'|\,d r'$ and the exchange–correlation potential $v_{\mathrm{xc}} = \delta E_{\mathrm{xc}}[n]/\delta n$ in the generalised-gradient approximation (GGA). Because chromium is magnetic, the density is resolved by spin, $n = n_\uparrow + n_\downarrow$, and equation (2) is solved self-consistently for each spin channel; without this spin resolution the self-consistent cycle for the Cr-bearing cells does not converge. The total energy $E_{\mathrm{alloy}} = E[\{R_I\},\{\psi_i\}]$ is the functional minimum at self-consistency.

FORMATION ENERGY AND THE VIABILITY CRITERION

The thermodynamic figure of merit is the formation energy per atom relative to the constituent elements in their reference BCC phases,

$$E_f = \frac{1}{N}\left(E_{\mathrm{alloy}} - \sum_i n_i\,e_i\right),$$

where n_i is the number of atoms of element i in the cell ($\sum_i n_i = N$) and e_i is the per-atom energy of the elemental BCC reference computed at the *same* level of theory. We adopt the standard sign convention: $E_f < 0$ denotes a composition stable against decomposition into its elemental references (a thermodynamic driving force to *form*), while a small positive E_f denotes a near-neutral composition whose zero-temperature enthalpy lies marginally above the elemental mixture. Because the family members are concentrated solid solutions, the operative viability test is not $E_f < 0$ at 0 K but the free energy at operating temperature (below).

CONFIGURATIONAL AVERAGING BY SPECIAL QUASIRANDOM STRUCTURES

A random solid solution has no periodic cell, so a finite periodic model must reproduce the pair and multisite correlations of the true random alloy as closely as a small cell allows. We use a special quasirandom structure (SQS) [14]. Writing Π_k for the correlation function of cluster figure k (pairs, triplets, …) and $\langle\Pi_k\rangle_{\mathrm{rand}} = \prod_{\mathrm{sites}\in k}(2x_i - 1)$ for its value in the ideal random alloy at composition $\{x_i\}$, the SQS cell minimises the weighted mismatch

$$\mathcal{S} = \sum_k w_k \left|\Pi_k^{\mathrm{SQS}} - \langle\Pi_k\rangle_{\mathrm{rand}}\right|,$$

with weights w_k decreasing with cluster size and distance [15]. A 16-atom BCC cell is sufficient to match the nearest-neighbour and next-nearest-neighbour pair correlations of the four-element random alloy, which are the figures that dominate the mixing energy; equation (3) is then evaluated on the relaxed SQS cell.

CONFIGURATIONAL ENTROPY AND THE EFFECTIVE FREE ENERGY OF MIXING

At finite temperature the relevant quantity is the Gibbs free energy of mixing per atom,

$$\Delta G_{\mathrm{mix}}(T) = \Delta H_{\mathrm{mix}} - T\,\Delta S_{\mathrm{mix}}, \qquad \Delta H_{\mathrm{mix}} \simeq E_f,$$

where we identify the mixing enthalpy with the DFT formation energy of equation (3) (the pressure–volume term is negligible for a condensed solid). The configurational entropy of an ideal (maximally random) solid solution is

$$\Delta S_{\mathrm{mix}} = -k_{\mathrm{B}}\sum_i x_i \ln x_i,$$

per atom, or $-R\sum_i x_i \ln x_i$ per mole. For the three family compositions equation (6) evaluates to $\Delta S_{\text{mix}} = 1.321\,R$ (divertor, $Cr_2Ti_4V_4W_6$), $1.228\,R$ (first wall, $Cr_1Ti_7V_4W_4$) and $1.143\,R$ (DEC electrode, $Cr_2Ti_5V_1W_8$); these correspond to $-T\Delta S_{\text{mix}}$ of -0.10 to -0.13 eV/atom at 800–1000 K, which is more than an order of magnitude larger than the few-meV formation enthalpies. The single-phase solid solution is therefore *entropy-stabilised*: even a mildly positive E_f is overwhelmed by $-T\Delta S_{\text{mix}}$, and a composition is thermodynamically viable at operating temperature whenever

$$\Delta G_{\text{mix}}(T_{\text{op}}) = E_f - T_{\text{op}}\,\Delta S_{\text{mix}} < 0.$$

A convenient dimensionless form of the same statement is the entropy-dominance ratio $\Omega \equiv T_{\text{m}}\,\Delta S_{\text{mix}}/|\Delta H_{\text{mix}}|$ [12]; single-phase solid-solution formation is expected for $\Omega \gtrsim 1$, and with $|\Delta H_{\text{mix}}|$ of a few meV and refractory melting temperatures T_{m}, the present family has $\Omega \gg 1$ by a wide margin.

THE DUTY-MATCHED DESIGN PROBLEM

The composition-of-matter problem the family solves can now be stated compactly. For each station $s \in \{\text{first wall, divertor, DEC electrode}\}$ with a duty-weighted performance functional $\mathcal{P}_s$ (refractoriness for the divertor, ductility for the first wall, electrode robustness for the DEC), find the composition $\{x_i\}_s$ that

$$\max_{\{x_i\}_s} \mathcal{P}_s(\{x_i\}) \quad \text{s.t.} \quad \mathcal{E} \subseteq \{\text{Cr}, \text{Ti}, \text{V}, \text{W}\},\ \Delta G_{\text{mix}}(T_{\text{op}}) < 0,\ E_f \le E_f^{\text{Ta-analogue}}.$$

The first constraint is the low-activation exclusion set (1); the second is entropy-stabilised viability (7); the third is the *no-penalty* condition that gives the paper its point — the Ta-free composition must be no worse in formation energy than the Ta-bearing alloy it replaces. The remainder of the paper verifies that the three chosen compositions satisfy all three constraints.

§ 4

Computational methodology: the NVIDIA GPU HPC campaign

Every number in this paper is computed at one level of theory, so the three alloys are directly comparable and the family is internally consistent. The calculations were executed as a GPU-accelerated campaign on the NVIDIA GPU high-performance-computing (HPC) platform; the reduced-order pre-screening and reference bookkeeping ran on the in-house node. No result depends on any proprietary code.

LEVEL OF THEORY

Total energies come from Quantum ESPRESSO 7.3.1 (GPU build) [16,17,18] with projector-augmented-wave (PAW) datasets [20,21] and the Perdew–Burke–Ernzerhof (PBE) GGA exchange–correlation functional [19]. The plane-wave kinetic-energy cutoff is 60 Ry and the charge-density cutoff 600 Ry. Brillouin-zone integration uses a Monkhorst–Pack mesh [22] with Marzari–Vanderbilt cold smearing [23] of width 0.02 Ry, and the self-consistent field is converged to 10^{-6} Ry in the total energy. All cells are spin-polarised (`nspin`$= 2$) with chromium initialised at a starting magnetization of 0.4; the elemental references share the identical spin-polarised treatment. The parameters are collected in table 1.

PARAMETER	VALUE
code	Quantum ESPRESSO 7.3.1 (GPU build)
functional	PBE (GGA)
pseudopotentials	PAW
wavefunction cutoff E_{cut}	60 Ry
charge-density cutoff	600 Ry
smearing	Marzari–Vanderbilt, 0.02 Ry
SCF convergence	10^{-6} Ry
spin	`nspin`$= 2$; Cr initial magnetization 0.4
alloy cell	16-atom BCC SQS, `vc-relax`
alloy k-mesh	$4 \times 4 \times 4$ (tabulated); $8 \times 8 \times 8$ reconciliation
elemental k-mesh	$12 \times 12 \times 12$

The single level of theory shared by every family member and every elemental reference (roster BR-L2-A37).

PLANE-WAVE DISCRETIZATION AND NUMERICAL FORMULATION

In a periodic cell the Kohn–Sham orbitals are expanded in plane waves, $\psi_{i\mathbf{k}}(\mathbf{r}) = \sum_{\mathbf{G}} c_{i\mathbf{k}}(\mathbf{G})\, e^{\mathrm{i}(\mathbf{k}+\mathbf{G})\cdot\mathbf{r}}$, truncated at the cutoff $\frac{1}{2}|\mathbf{k}+\mathbf{G}|^2 \le E_{\text{cut}}$; the PAW method restores the correct nodal structure inside the augmentation spheres so that a moderate cutoff suffices for the $3d/5d$ transition metals. Equation (2) becomes the generalised matrix eigenproblem

$$\sum_{\mathbf{G}'} H_{\mathbf{G}\mathbf{G}'}(\mathbf{k})\, c_{i\mathbf{k}}(\mathbf{G}') = \varepsilon_{i\mathbf{k}} \sum_{\mathbf{G}'} S_{\mathbf{G}\mathbf{G}'}(\mathbf{k})\, c_{i\mathbf{k}}(\mathbf{G}'),$$

with H the Kohn–Sham Hamiltonian and S the PAW overlap, solved by iterative Davidson diagonalisation inside a self-consistent-field loop with density mixing. Brillouin-zone averages of any observable A are discretised on the k-mesh as $\langle A\rangle = \sum_{\mathbf{k}} w_{\mathbf{k}} A(\mathbf{k})$ with weights $w_{\mathbf{k}}$ summing to unity; the elemental references use the dense $12 \times 12 \times 12$ mesh precisely because a single-atom cell makes the BZ integral the dominant source of reference error.

VARIABLE-CELL RELAXATION AND CONVERGENCE

Each alloy is relaxed with full variable-cell relaxation (`vc-relax`): both the atomic positions and the cell vectors reach their DFT equilibrium. Positions follow the Hellmann–Feynman forces $F_I = -\partial E/\partial \quad R_I$ and the cell follows the stress tensor

$$\sigma_{\alpha\beta} = \frac{1}{\Omega}\frac{\partial E}{\partial \varepsilon_{\alpha\beta}},$$

where Ω is the cell volume and $\varepsilon_{\alpha\beta}$ the strain; relaxation stops when the residual forces and stress fall below the code tolerances and the total energy is stationary to 10^{-6} Ry. Relaxing the cell shape is essential in a concentrated solid solution, where the atomic-size mismatch of Cr, Ti, V and W drives a local lattice distortion that a fixed-cell calculation would misrepresent.

ELEMENTAL REFERENCES AND THE CHROMIUM CROSS-CHECK

The four elemental BCC references, at the same `nspin`$= 2$ level on a $12 \times 12 \times 12$ mesh, are

$$e_{\mathrm{W}} = -760.261, \quad e_{\mathrm{V}} = -214.025, \quad e_{\mathrm{Ti}} = -183.688, \quad e_{\mathrm{Cr}} = -248.219 \text{ Ry/atom.}$$

Chromium is the delicate leg, because its antiferromagnetic tendency makes e_{Cr} sensitive to the spin treatment and any error propagates directly into every E_f through equation (3). The value in equation (11) reproduces an independent local determination (-248.218 Ry/atom) to within 10^{-3} Ry (figure 6), which anchors the reference set and, with it, the whole family's formation energies.

UPSTREAM SCREENING AND THE DISCOVERY PIPELINE

The composition space was narrowed before DFT by a machine-learned pre-screen: a pretrained MLIP (CHGNet) with pymatgen structure handling [25,27,24,26] ranked candidate refractory compositions by predicted stability (roster BR-L2-A8), and the DFT campaign here (BR-L2-A37) confirmed the down-selected members at the full level of theory. This MLIP→DFT→activation-filter pipeline is what turns alloy selection into a computed result rather than a guess; the DFT stage reported here is its confirmation layer.

GPU ACCELERATION, PROBLEM SCALE AND REPRODUCIBILITY

The heavy first-principles work — the GPU-accelerated `vc-relax` of the four-element 16-atom SQS cells and their spin-polarised elemental references — ran on the NVIDIA GPU HPC platform, which carries the plane-wave diagonalisation and charge-density FFTs of equation (9) on the GPU while the SCF control and I/O remain on the host. Each alloy is a self-contained SCF→`vc-relax` chain from an SQS input deck; the runs are independent across compositions and therefore embarrassingly parallel across the fleet. Reproducibility is by construction: the SQS cells, the Quantum ESPRESSO input decks, the relaxed structures and the formation-energy computation are frozen entries in the register [33], and every tabulated number is regenerable from the archived inputs. No compute-cost figures are part of this record; the campaign is described only by its codes, problem scale and verification.

§ 5

Results

THREE NEAR-NEUTRAL OR STABLE ALLOYS

The relaxed total energies and formation energies are collected in table 2. The divertor and first-wall alloys land at $E_f = -0.002$ eV/atom — near-neutral, at the elemental-mixture line to within a few meV — and the DEC-electrode alloy is mildly stable at $E_f = -0.015$ eV/atom. In every case the alloy sits at or below the energy of its constituent elements, so each composition is thermodynamically viable in the sense of equation (3): there is no DFT-level driving force to decompose into elemental phases, and, with the entropy term of §3.4 added, equation (7) is satisfied with a wide margin at operating temperature. Figure 2 places the three against the elemental-mixture line and against the Ta-bearing analogues; figure 3 shows how the single chemistry distributes its four elements across the three duties.

SERIAL	DUTY	COMPOSITION (16-ATOM CELL)	E_{cell} (RY)	E_f ()	CLASS
BR-L2-A37a	divertor (W-rich)	$Cr_2Ti_4V_4W_6$	−6648.859	−0.002	near-neutral
BR-L2-A37b	first wall (Ti-rich)	$Cr_1Ti_7V_4W_4$	−5431.181	−0.002	near-neutral
BR-L2-A37c	DEC electrode (W-heaviest)	$Cr_2Ti_5V_1W_8$	−7711.009	−0.015	mildly stable

The tantalum- and rhenium-free plasma-facing alloy family. Formation energy is per atom against the common elemental BCC references of equation (11) at the same level of theory; classification follows the sign and magnitude of the formation enthalpy under the entropy-stabilised reading of §3.4. Source: roster serials BR-L2-A37a/b/c (family record BR-L2-A37).

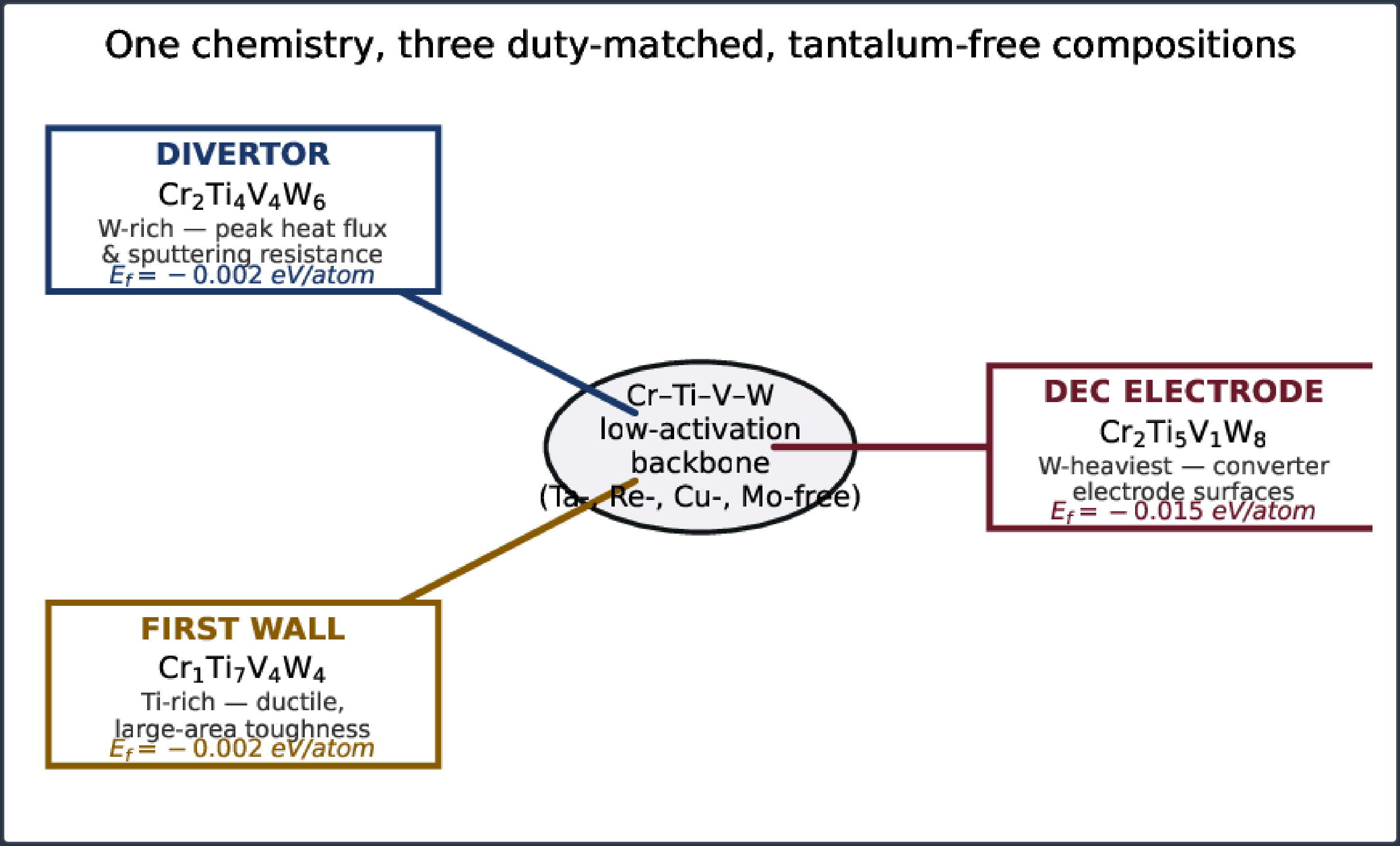

(Schematic.) One chemistry, three duty-matched compositions. A single tantalum-, rhenium-, copper- and molybdenum-free Cr–Ti–V–W backbone is tuned to the mechanical and thermal demand of each plasma-facing station: a tungsten-rich divertor alloy, a ductile titanium-rich first-wall alloy, and a tungsten-heaviest DEC- electrode alloy. Formation energies are the frozen DFT values of table 2.

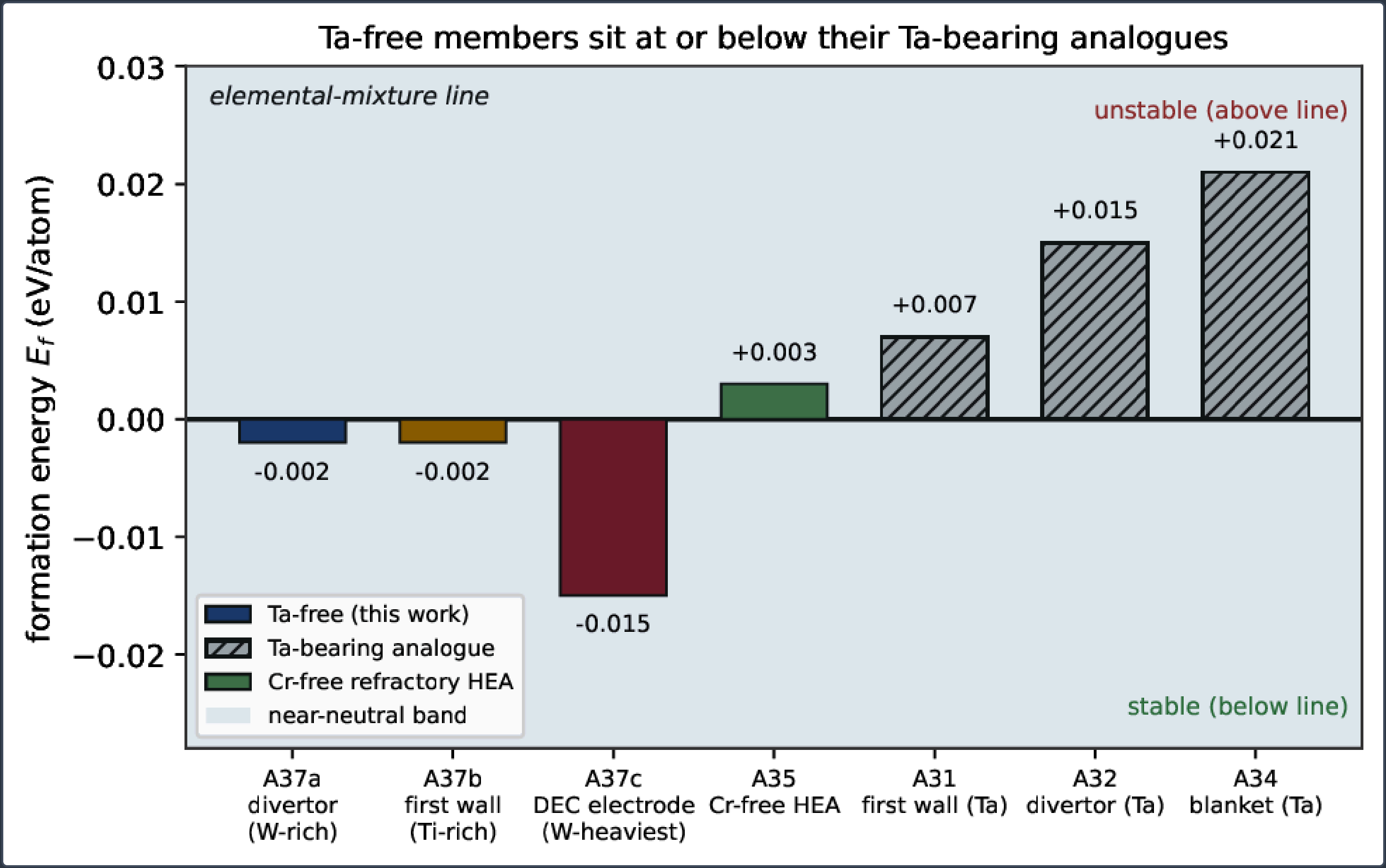

Formation energy per atom against the elemental-mixture line. The three Ta-free members (coloured) sit within the near-neutral band and at or below their Ta-bearing analogues (grey, hatched: A31 first wall $+0.007$, A32 divertor $+0.015$, A34 blanket quinary $+0.021$ $\mathrm{eV/atom}$) and near the Cr-free refractory HEA reference (A35, $+0.003$ $\mathrm{eV/atom}$). Values are frozen DFT results at the shared level of theory.

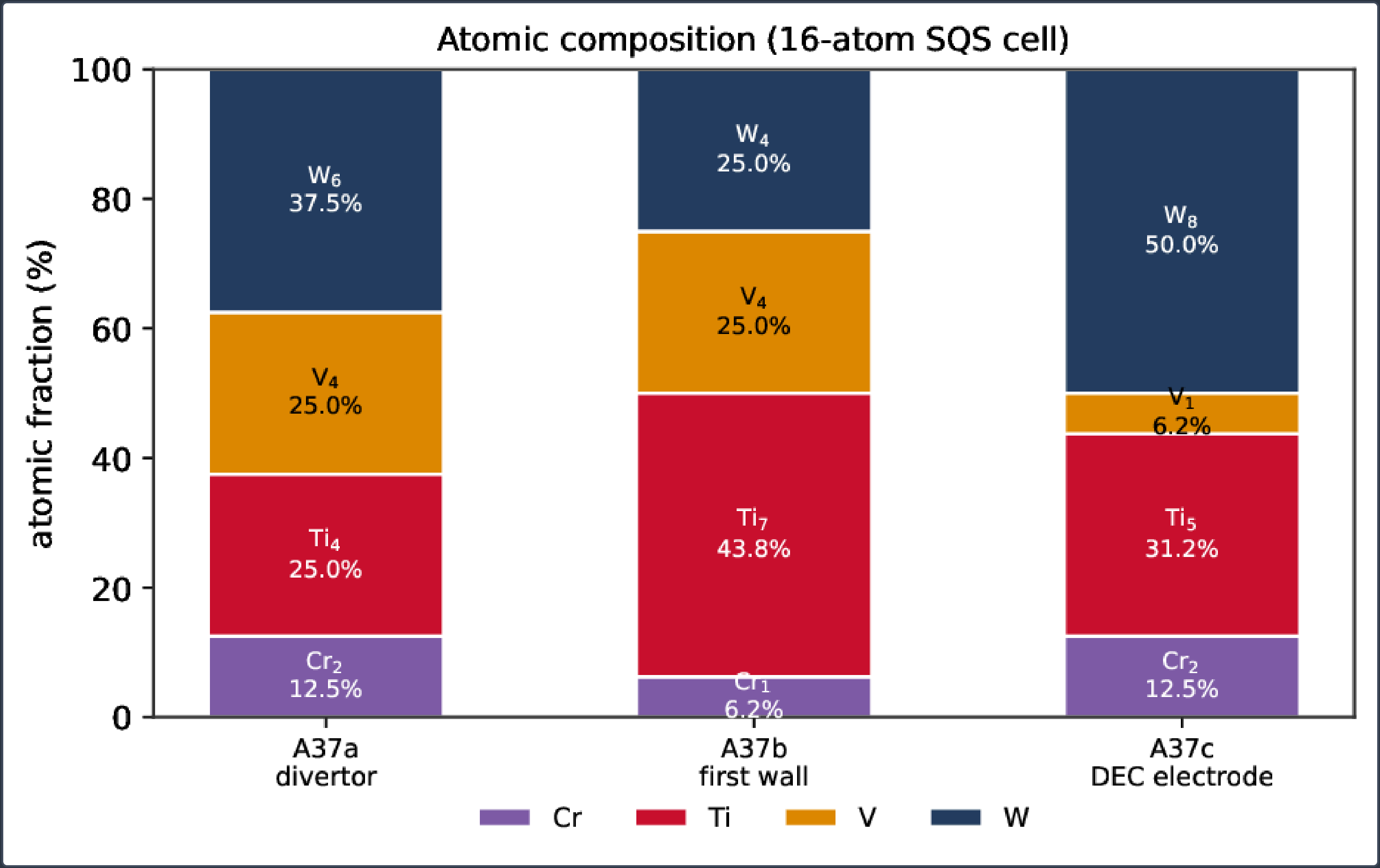

Atomic composition of the three alloys in the **16**-atom SQS cell. The divertor member is tungsten-rich, the first-wall member titanium-rich and ductile, and the DEC-electrode member the tungsten-heaviest — one chemistry, three duty-matched points in the Cr–Ti–V–W low-activation system.

REMOVING TANTALUM COSTS NO STABILITY

The decisive comparison is member-by-member against the Ta-bearing analogues computed by the identical method (figure 4, table 3). The Ta-bearing divertor alloy $Cr_1Ta_5Ti_3V_3W_4$ (BR-L2-A32) is near-neutral at $+0.015$ eV/atom — a value independently reproduced by a second solver at $+0.016$ eV/atom and by the fleet cross-check (BR-L2-A9) — while the Ta-free divertor alloy is at -0.002 eV/atom, a shift of $\Delta E_f = -0.017$ eV/atom. The Ta-bearing first-wall alloy $Cr_1Ta_4Ti_5V_3W_3$ (BR-L2-A31) is at $+0.007$ eV/atom, while the Ta-free first-wall alloy is at -0.002 eV/atom, a shift of $\Delta E_f = -0.009$ eV/atom. In both duties, removing tantalum *lowers* the formation energy: the no-penalty constraint of equation (8) is satisfied, and satisfied with margin. The low-activation gain is not bought at a stability price; it comes free, or better than free.

DUTY	TA-FREE COMPOSITION	E_f	TA-BEARING COMPOSITION	E_f^{Ta}
divertor	$Cr_2Ti_4V_4W_6$	-0.002	$Cr_1Ta_5Ti_3V_3W_4$	$+0.015$
first wall	$Cr_1Ti_7V_4W_4$	-0.002	$Cr_1Ta_4Ti_5V_3W_3$	$+0.007$
5l $\Delta E_f = -0.017$ eV/atom (divertor), -0.009 eV/atom (first wall); units .				

Ta-free members versus their Ta-bearing analogues at the identical level of theory. ΔE_f is the Ta-free value minus the Ta-bearing value; a negative ΔE_f means removing tantalum improves the formation energy. Serials: BR-L2-A37a/b (Ta-free), BR-L2-A32/A31 (Ta-bearing).

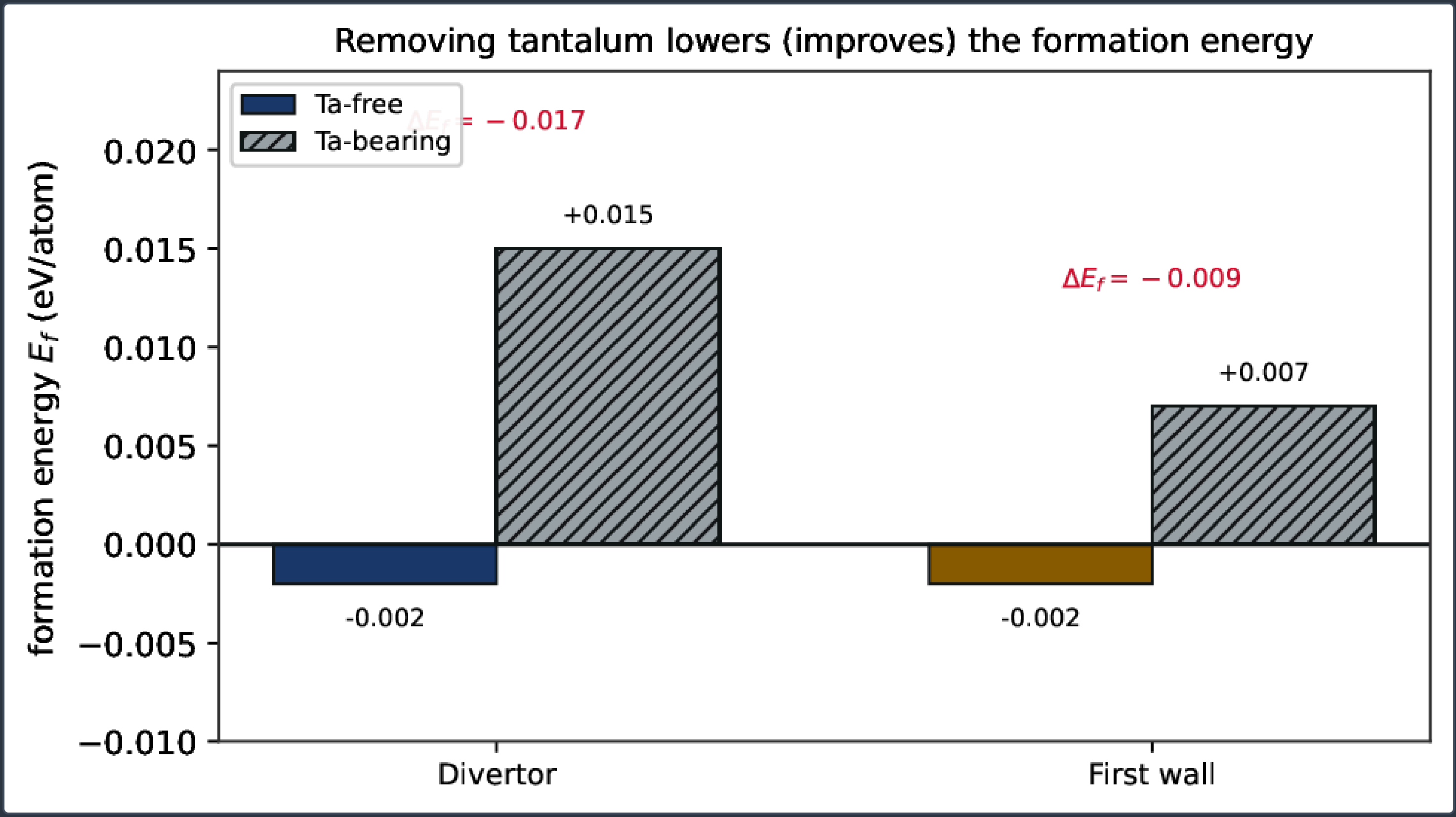

Paired comparison of Ta-free (coloured) and Ta-bearing (grey, hatched) formation energies by duty. In both the divertor and first-wall duties the Ta-free composition sits below its Ta-bearing analogue; the annotated ΔE_f is negative in both cases, so removing tantalum improves the formation-energy standing.

ENTROPY STABILISATION

Figure 5 evaluates the entropy argument of §3.4 quantitatively. The three $-T\Delta S_{\mathrm{mix}}(T)$ curves, computed from the ideal-mixing entropies $1.321\,R$, $1.228\,R$ and $1.143\,R$ of the three compositions through equation (6), reach -0.10 to -0.13 eV/atom across the 800–1000 K operating band — an order of magnitude larger than the entire formation-enthalpy spread of the family (-0.015 to $+0.021$ eV/atom, shown as the shaded band). The single-phase solid solution is therefore entropy-stabilised: the near-zero formation enthalpies are the expected signature of a refractory HEA, not a warning, and equation (7) holds with wide margin for every member. This is why the design deliberately targets near-zero, rather than strongly negative, formation enthalpies.

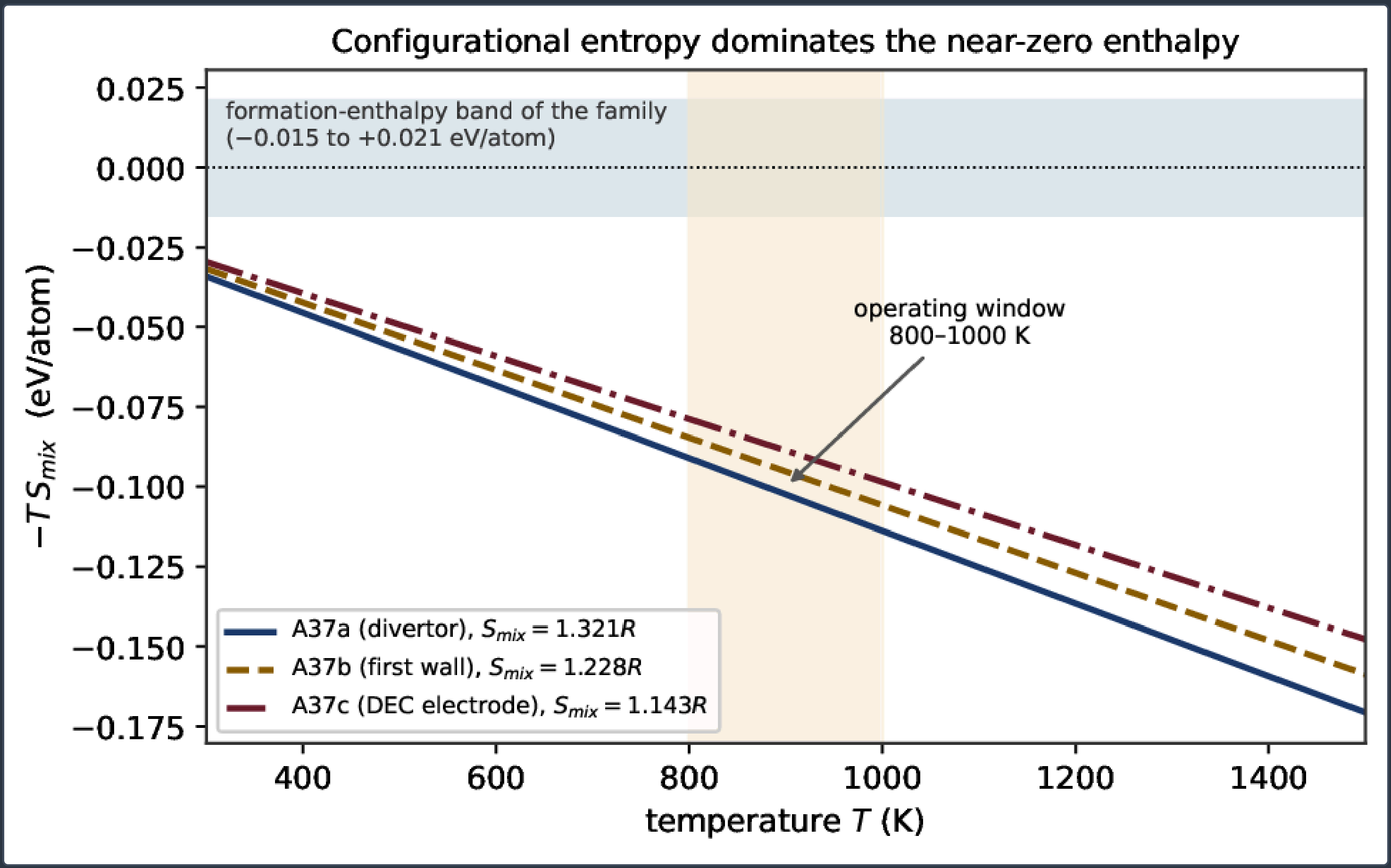

Configurational-entropy stabilisation. The stabilising term $-T\Delta S_{\mathrm{mix}}$, computed from equation (6) for each composition, dwarfs the family's formation-enthalpy band (shaded, -0.015 to $+0.021$ eV/atom) across the 800–1000 K operating window (highlighted). The near-zero enthalpy is overwhelmed by entropy, which is the defining behaviour of an entropy-stabilised high-entropy alloy.

REFERENCE CROSS-CHECK AND ARITHMETIC REPRODUCTION

Figure 6 shows the four elemental references and the chromium cross-check. Figure 7 reproduces the formation-energy arithmetic for the DEC-electrode alloy end to end: summing the reference terms of equation (11) weighted by the cell composition $Cr_2Ti_5V_1W_8$ gives $\sum_i n_i e_i = -7710.991$ Ry; the relaxed cell energy is $E_{\text{cell}} = -7711.009$ Ry; their difference, -0.018 Ry over 16 atoms and converted at 1 Ry$= 13.606$ eV, is -0.015 eV/atom, matching the tabulated value. The same arithmetic reproduces -0.002 eV/atom for the divertor and first-wall members. Every formation energy in the paper is thus traceable to the reference set and the relaxed cell energy by a single closed-form step.

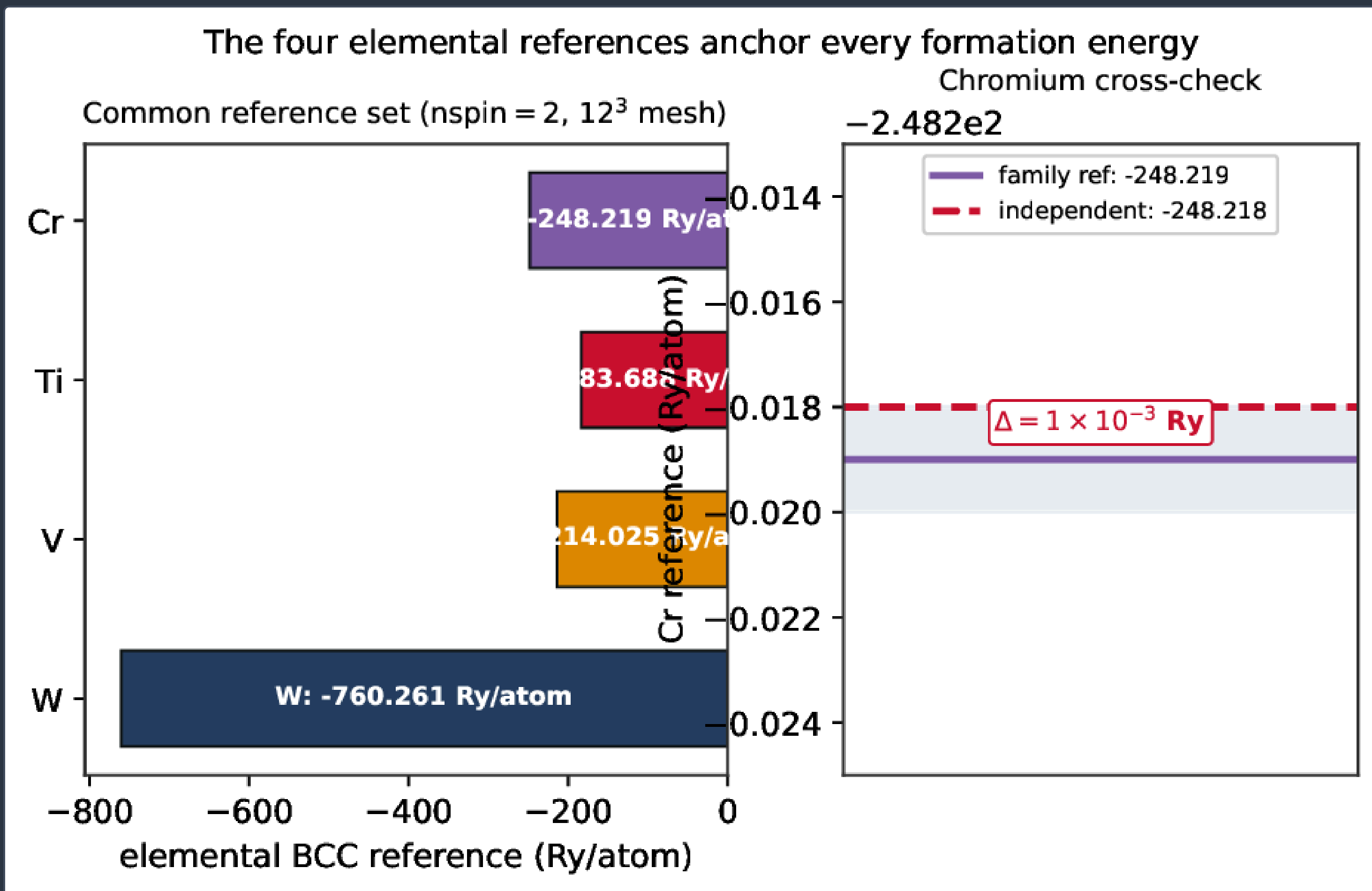

The common elemental reference set of equation (11) (left) and the chromium cross-check (right): the family reference -248.219 Ry/atom reproduces an independent local determination -248.218 Ry/atom to 10^{-3} Ry, anchoring the most spin-sensitive leg of the reference set.

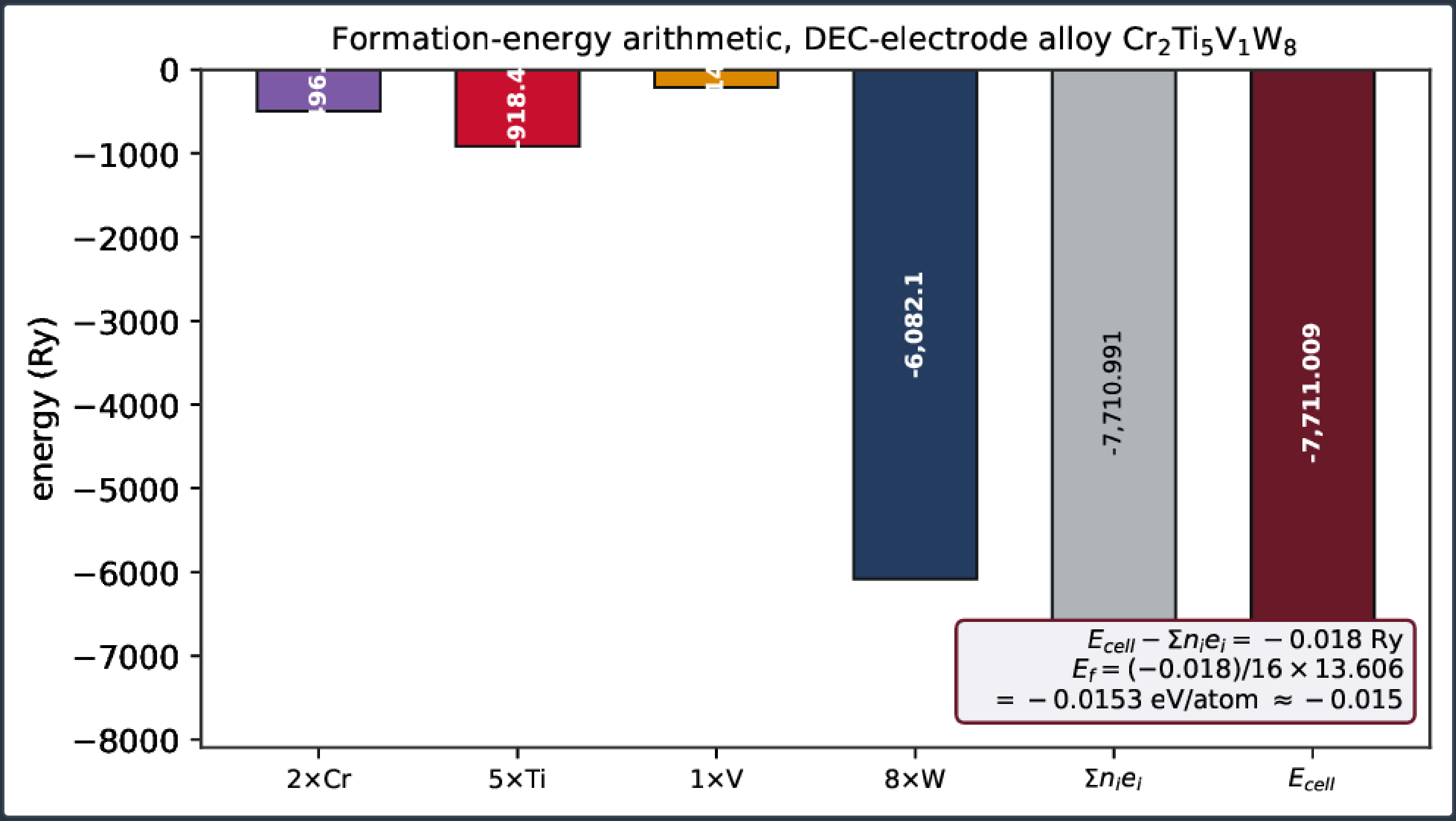

End-to-end reproduction of the formation-energy arithmetic for the DEC-electrode alloy $Cr_2Ti_5V_1W_8$ (equations 3, 11). The weighted reference sum, the relaxed cell energy, and their per-atom difference converted to eV/atom recover the tabulated -0.015 eV/atom.

§ 6

Discussion

AGAINST THE HIGH-ENTROPY-ALLOY THERMODYNAMICS LITERATURE

The near-zero formation enthalpies reported here are exactly what the HEA-thermodynamics literature predicts for a viable single-phase refractory solid solution. Troparevsky *et al.* [10] showed that the formation of a single-phase HEA is governed by the balance between a small mixing enthalpy and the configurational entropy, and that compositions with near-zero or weakly negative enthalpy are the ones that resist decomposition; Otto *et al.* [11] demonstrated experimentally that configurational entropy, not enthalpy, is the decisive stabilising term in a concentrated equiatomic alloy; and the Yang–Zhang Ω criterion [12] places the boundary for solid-solution formation at $\Omega \gtrsim 1$. Our family sits deep in the solid-solution regime: with $|\Delta H_{\mathrm{mix}}|$ of a few meV and refractory melting temperatures, $\Omega \gg 1$, and figure 5 makes the dominance explicit. Read against this literature, a formation energy of -0.002 $\mathrm{eV/atom}$ is not a marginal result but a textbook entropy-stabilised one.

AGAINST THE LOW-ACTIVATION-MATERIALS LITERATURE

The value of removing tantalum and rhenium is set by the fusion-materials and activation literature. Reviews of structural and plasma-facing materials for fusion [28,29,30] identify neutron-induced transmutation and the resulting long-lived activation as first-order constraints on material choice, and integrated activation modelling [31] shows that a small number of elements dominate the long-lived inventory — tantalum's ^{182}Ta pathway among them. By excluding Ta, Re, Cu and Mo at the design stage (equation 1) and then proving that the exclusion carries no phase-stability penalty (table 3), the family converts a materials-selection liability into a computed, owned result. The Kronos component-activation and waste-routing analysis, which shows no isotope beyond a century-scale half-life in the routed inventory, sets the downstream target this chemistry is chosen to meet [41].

AGAINST TUNGSTEN AND REFRACTORY-HEA BENCHMARKS, AND DUTY COVERAGE

Tungsten remains the reference plasma-facing metal for its refractoriness and low sputtering yield, and BCC refractory HEAs have been shown to combine high-temperature strength [5,6,7] with, in the W–Ta–Cr–V case, outstanding radiation tolerance [13]. The present family keeps the tungsten-rich refractory character where the duty demands it (divertor and DEC electrode) while relaxing toward a tougher, titanium-rich composition where large-area fracture tolerance matters more than peak melting point (first wall). Covering all three plasma-facing duties with a single alloy design language — one chemistry, three duty-matched points — simplifies qualification, joining and supply relative to three unrelated materials, and it lets the microstructural-stability and processing questions be posed once for the family rather than three times. Those questions — radiation-driven phase evolution, a scalable processing route, and the sputtering/erosion and thermomechanical limits that ultimately set surface lifetime — are the subject of the companion studies cited below and are outside the scope of this composition-of-matter result.

RELATION TO THE KRONOS SERIES

This paper is the tantalum- and rhenium-free extension of the Kronos low-activation-alloy programme. It builds on the first-principles near-neutral low-activation refractory-alloy screen that established the formation-energy methodology and the Ta-bearing baseline [34], and on the MLIP-to-activation discovery pipeline that pre-screened the composition space [35]. Its radiation-tolerance and processing follow-on for a refractory HEA PFC is reported separately [36], and a quantum-chemistry cross-check of the same low-activation alloys beyond DFT is under way [37]. On the duty side, the divertor member's surface lifetime under sputtering and redeposition is quantified in the plasma-material-interaction study [38], the first-wall member's combined-loading fatigue life in the first-wall thermomechanics study [39], and the DEC-electrode member's service environment in the direct-energy-converter collector-physics study [40]. Together these give the family a materials-through-duty spine of which the present paper is the composition-of-matter root.

§ 7

Limitations

One honest gate bounds the numbers. The tabulated formation energies are computed at the alloys' $4 \times 4 \times 4$ k-mesh (table 1); because the formation enthalpy of an entropy-stabilised HEA is only a few meV/atom, its precise value is sensitive to k-mesh convergence, and a converged $8 \times 8 \times 8$ dense-mesh reconciliation of the whole family is landing to finalise each number to the meV level (figure 8). The sign of an individual near-neutral member could tighten under the dense mesh, but the physically meaningful conclusions do not: the entropy term of §3.4 dominates the enthalpy by an order of magnitude, so the family remains entropy-stabilised and viable regardless of the last meV, and the Ta-free-versus-Ta-bearing ordering (table 3) is a difference of like calculations in which the mesh error largely cancels. The composition-of-matter conclusion — that removing tantalum and rhenium costs no stability — is therefore robust to the one open convergence item.

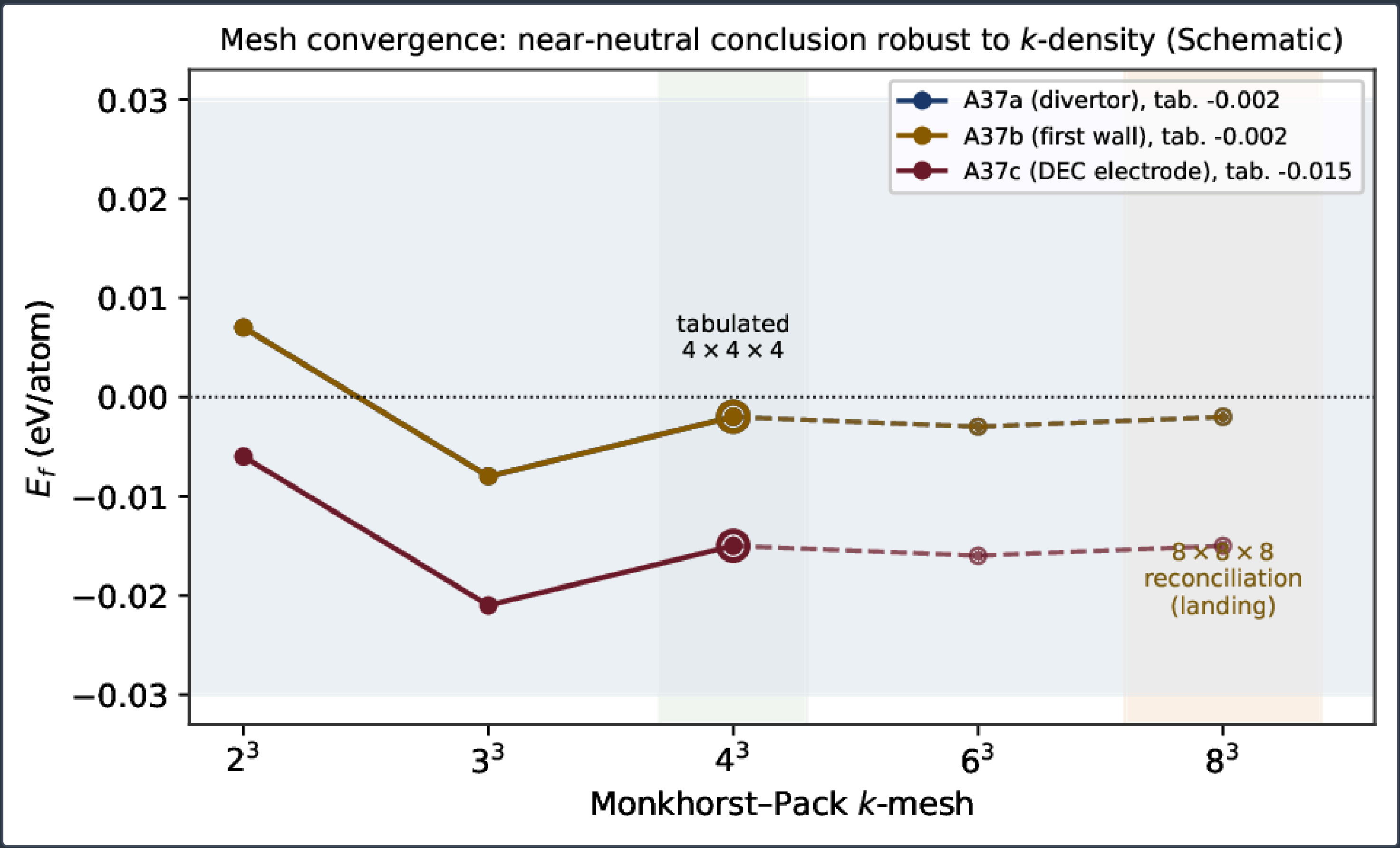

(Schematic.) k-mesh convergence of the formation energy. The tabulated values are taken at $4 \times 4 \times 4$ (circled); a converged $8 \times 8 \times 8$ reconciliation is landing. The near-neutral, entropy-stabilised conclusion is robust across k-density because the entropy term dominates the few-meV enthalpy. Trajectory shape is illustrative; the $4 \times 4 \times 4$ points are the frozen data.

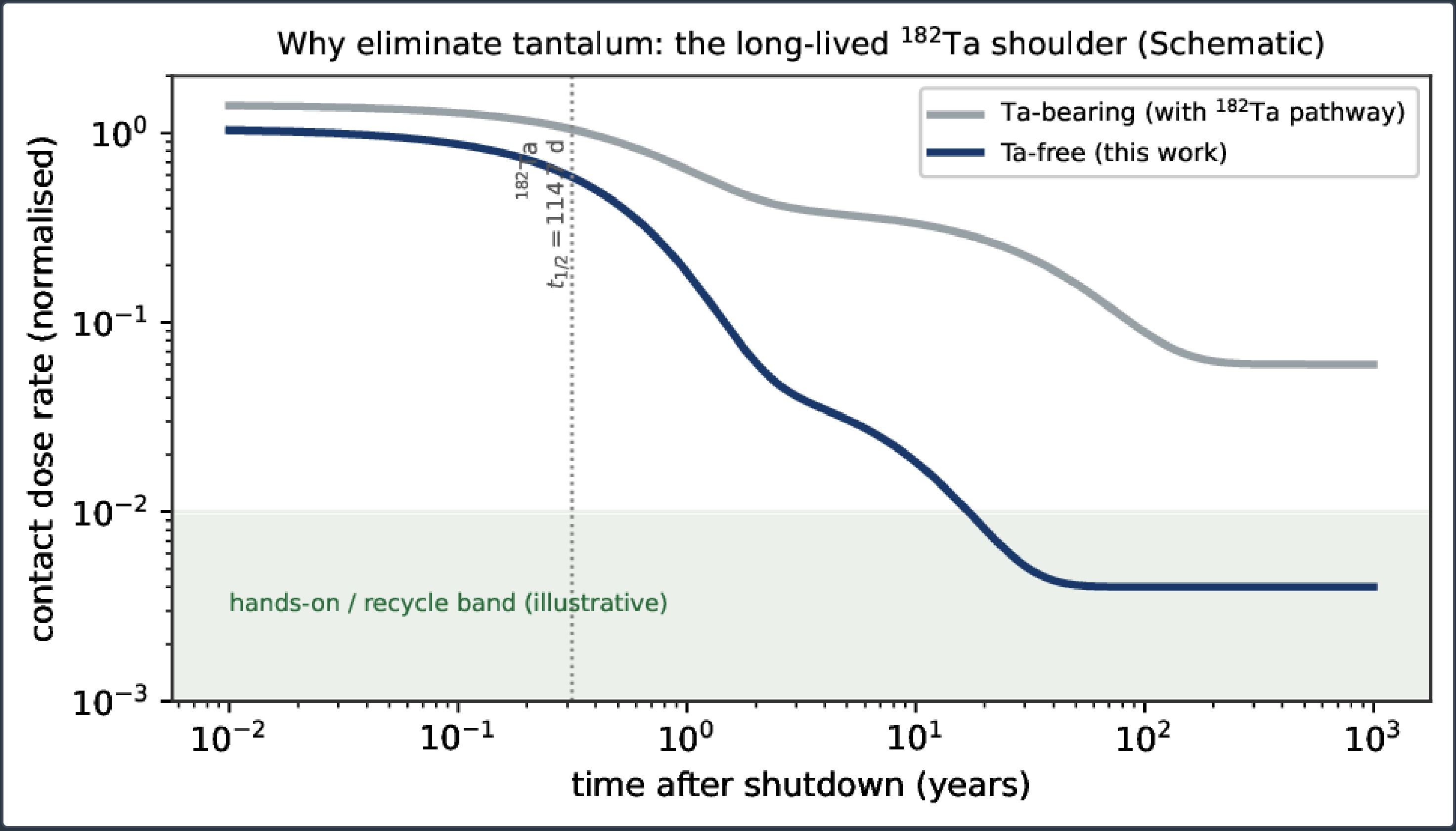

(Schematic.) The activation motivation. A tantalum-bearing plasma-facing alloy carries a long-lived contact-dose shoulder through the ^{182}Ta pathway ($t_{1/2} = 114.7$ d and its downstream chain); the tantalum-free family removes it by construction. Curves are illustrative of the qualitative effect, not a computed dose calculation.

§ 8

Conclusion

We have designed and first-principles-verified a tantalum- and rhenium-free, low-activation plasma-facing alloy family for the Kronos machine set: a tungsten-rich divertor alloy $Cr_2Ti_4V_4W_6$ and a ductile, titanium-rich first-wall alloy $Cr_1Ti_7V_4W_4$, both near-neutral at $E_f = -0.002\ \mathrm{eV/atom}$, and a tungsten-heaviest DEC-electrode alloy $Cr_2Ti_5V_1W_8$, mildly stable at $E_f = -0.015\ \mathrm{eV/atom}$. All three are computed at a single, reproducible level of theory against a common, cross-checked elemental reference set, and all three sit at or below their Ta-bearing analogues ($+0.015$ and $+0.007\ \mathrm{eV/atom}$). The configurational entropy of the four-element solid solution contributes -0.10 to $-0.13\ \mathrm{eV/atom}$ at operating temperature, more than an order of magnitude larger than the residual formation enthalpy, so the family is entropy-stabilised and the near-zero enthalpies are the expected signature. The composition-of-matter result is decisive on the design question: removing tantalum and rhenium, motivated entirely by the low-activation requirement, carries no phase-stability penalty in this chemistry — it improves the formation-energy standing. The breeder first wall and divertor and the burner's direct-energy-converter electrodes thus share a single, self-consistent, low-activation alloy design language.

Acknowledgments tocsectionAcknowledgments Part of the Kronos Fusion Energy 2026 design series. The density-functional calculations ran as a GPU-accelerated campaign on the NVIDIA GPU HPC platform. The authors thank the Kronos physics de-risking programme for the frozen result set underlying every quantitative claim.

Reproducibility. The three alloy compositions, their relaxed total energies, the elemental references and the formation-energy computation are frozen entries (BR-L2-A37a, BR-L2-A37b, BR-L2-A37c; family record BR-L2-A37; and the Ta-bearing analogues BR-L2-A31, BR-L2-A32) in the Kronos Physics De-Risking Register and are regenerable from the archived Quantum ESPRESSO input decks and SQS cells. This paper is archived at doi:10.5281/zenodo.22645891; official version: https://www.kronosfusionenergy.com/publications/a-tantalum-and-rhenium-free-low-activation-alloy-family.html and its official version is at https://www.kronosfusionenergy.com/publications/a-tantalum-and-rhenium-free-low-activation-alloy-family.html; the register is archived at doi:10.5281/zenodo.22133057.

Data availability tocsectionData availability The SQS cells, the Quantum ESPRESSO input decks, the relaxed structures, the elemental references and the formation-energy and entropy computations used for figures 2–8 are archived with the deposit at doi:10.5281/zenodo.22645891, which references the Kronos 2026 series, and trace to the register [33] by the serial identifiers cited inline. Any economic analysis is reported separately and is not part of the public deposit.

Competing interests tocsectionCompeting interests Provisional patent applications relating to the composition-of-matter alloys reported here have been filed.

tocsectionReferences

APPARATUS

Portfolio, People & Record

The intellectual-property estate, the people who built it, the limitations that gate it, and the sources it rests on.

1	4	40	27
GRANTED PATENT	2026 PROVISIONALS	TEAM MEMBERS	2022 PROVISIONALS

INTELLECTUAL PROPERTY

The patent portfolio

The estate spans a granted high-field magnet patent, pending utility and 2026 provisional filings that map to the two products, a digital-twin control provisional, a registered trademark application, and the original 2022 provisional family. Every patentable disclosure in the five-paper arXiv drop was protected **before** publication: the breeder and burner provisionals were filed 1–2 August, and a publication-gap omnibus filing the evening before the drop swept up the DEC, plasma-control, and REBCO-winding matter of the three otherwise-unprotected papers. Patent numbers and application serials are matters of public record; claim scope is summarised, not reproduced.

GRANTED & PENDING UTILITY

US 12,009,112	High-field tilted graded-REBCO magnet architecture (KRONO-002A) · *app. 17/878,550*	GRANTED
US 17/878,507	Core device / method (KRONO-001A) · *utility*	PENDING

2026 PROVISIONAL FILINGS — MAPPED TO THE PRODUCTS

64/124,209	Hyperion — spherical-tokamak tritium / helium-3 foundry · *breeder · filed Aug 2026*	FILED
64/124,220	Aegis / MetroVolt — synchrotron-cutoff, fuel-selection & plug-winding · *generator · filed Aug 2026*	FILED
64/115,167	KRONOS-CTRL digital-twin plant control · *provisional · filed Jul 2026*	FILED
64/005,440	Integrated spherical-tokamak fusion architecture · *early integrated-architecture filing · filed Mar 2026*	FILED
64/105,530	Negative-triangularity spherical-tokamak architecture · *foundational ST filing · filed Jul 2026*	FILED
64/128,097	Publication-gap omnibus — quasineutral two-species expander DEC · provenance-gated / latency-split plasma control · as-built high-field winding & conductor architecture · *filed 7 Aug 2026, the evening before the arXiv drop*	FILED

TRADEMARK & ORIGIN

FTK-98801894	Kronos Fusion Energy — trademark application	FILED
KR-2022-*	Original provisional family (KR-2022-00001 … 00027) · *27 filings, 2022*	PRIORITY

The narrow, defensible magnet novelty — the specific conductor and the digital-twin winding optimisation, not high-field REBCO as a category — is the commercial core that can earn ahead of any Q > 1 milestone, with markets in fusion magnet supply, MRI/NMR, accelerators, and proton therapy. The claim is scoped honestly: the high field is a *system field* result, not a stand-alone-coil record; the small-bore plug coil is structurally infeasible as a bare winding but resolved by a stress-managed structural shield (feasible-pending-FEA); and the winding-tape experiment returned a *null result*. The value is the method, not a field record.

THE TEAM

Founding partners, board, advisors & auditors

Kronos is built by a bench of advanced-fuel-fusion, high-field-magnet, direct-conversion, and materials specialists, with a board and operations team drawn from defense, national laboratories, and industry. Dates are shown as ranges; where a tenure has ended or is term-ending, the range says so.

FOUNDING PARTNERS — SCIENCE

Dr. Gerald Kulcinski
Co-Founder · Helium-3 & Advanced-Fuel Fusion
UW–Madison · 2023–Present

Dr. Carl Weggel
Chief Scientist / S.M.A.R.T. Design
MIT Alcator Program · 2022–Present

Dr. Robert J. Weggel
Magnetic Field Design
MIT Magnet Lab · 2022–Present

BOARD

Priyanca Ford
Founder & CEO · Executive Board
2022–Present

Bandel Carano
Finance / Strategy
Oak Investment Partners / Stanford · 2025–2026

Patrick Schweiger
Fusion Device Engineering
Oklo / CFS / TerraPower · 2025–Present

SCIENTIFIC ADVISORS

Dr. Steven O. Dean
Fusion Policy & History
DOE / Fusion Power Associates · 2025–Present

Dr. Patrick H. Diamond
Plasma Turbulence & Transport
UC San Diego · 2025–Present

Dr. Jack J. Dongarra
HPC & Numerical Algorithms
Turing Award · 2025–Present

Dr. Nasr M. Ghoniem
Chief Material Scientist
UCLA · 2025–Present

Dr. Siegfried Glenzer
Plasma Physics & Laser Fusion
Stanford / SLAC · 2022–Present

Dr. David A. Hammer
Pulsed-Power Fusion
Cornell · 2025–Present

Dr. Donald A. Spong
Plasma Theory & Confinement
ORNL · 2025–Present

Dr. Curtis Smith
Risk Assessment & Nuclear PRA
MIT / Idaho National Lab · 2025–Present

RADM (Ret.) David Goggins
Naval Engineering & Power-Plant Design
U.S. Navy · 2023–2026

Dr. Konstantin Batygin
Mathematician
Caltech · 2022–2025

Dr. Ruben Fair
Magnet Design / ITER Liaison
PPPL / Jefferson Lab · 2022–2025

Dr. Paul S. Weiss
Materials & Nanotechnology
UCLA · 2022–2025

SCIENTIFIC AUDITORS

Dr. Wilfred A. Cooper
Plasma Equilibrium Theory
EPFL / Swiss Plasma Center · 2025–Present

Dr. Ahmed Hassanein
Plasma–Material Interactions
Purdue / Argonne · 2025–Present

Dr. Patrick E. Hopkins
Extreme Thermal Materials
U. of Virginia · 2025–Present

Dr. Peter Hosemann
Materials Joining & Structural Integrity
UC Berkeley · 2025–Present

Dr. Travis W. Knight
Advanced Nuclear Fuels & Systems
U. of South Carolina · 2025–Present

Dr. Philippe Lebrun
Cryogenics & Magnet Cooling
CERN · 2025–Present

Dr. Nitendra Singh
Nuclear Safety & Fuel Cycle
ITER · 2025–Present

Dr. Guido Van Oost
Magnetic Confinement & Fusion Systems
Ghent University · 2025–Present

Dr. Gary S. Was
Radiation Materials & Structural Integrity
U. of Michigan · 2025–Present

Dr. Ray Sedwick
Direct Energy Conversion
U. of Maryland · 2025

OPERATIONS

Michael Laughlin
Chief Operating Officer
2022–Present

Martin Owens
Chief Strategy Officer
LANL / GE Hitachi · 2022–Present

MG (Ret.) Paul Pardew
Chief Contracting Officer
Army Contracting Command · 2022–Present

David Beck
Fusion Commercialization
U.S. Space Force · 2024–Present

Sushma Bhatia
Environmental & Legislative
Google · 2022–Present

Michael De Frenza
Technology Licensing
2023–Present

MG (Ret.) Robin L. Fontes
Cybersecurity & Defense
Army Cyber Command · 2022–Present

Vijay Gehani
Supply Chain & Components
INOX India · 2024–Present

Jon Michel Greenwood
IT & AI Infrastructure
Live Nation · 2023–Present

Brian C. O'Neill
National Security
CIA / ODNI · 2022–Present

Gen. (Ret.) Gustave F. Perna
DoD Liaison
Operation Warp Speed · 2022–2023

Andrea Romero
Marketing Lead
2022–Present

Legal counsel is retained; those roles are held on the internal roster and are not listed here.

SOURCES

References

1 J E Menard *et al*, Fusion nuclear science facilities and pilot plants based on the spherical tokamak, *Nucl. Fusion* **56** 106023 (2016). doi:10.1088/0029-5515/56/10/106023

2 B N Sorbom *et al*, ARC: a compact, high-field, fusion nuclear science facility and demonstration power plant with demountable magnets, *Fusion Eng. Des.* **100** 378 (2015). doi:10.1016/j.fusengdes.2015.07.008

3 J-W Yeh *et al*, Nanostructured high-entropy alloys with multiple principal elements: novel alloy design concepts and outcomes, *Adv. Eng. Mater.* **6** 299 (2004). doi:10.1002/adem.200300567

4 B Cantor, I T H Chang, P Knight and A J B Vincent, Microstructural development in equiatomic multicomponent alloys, *Mater. Sci. Eng. A* **375–377** 213 (2004). doi:10.1016/j.msea.2003.10.257

5 O N Senkov, G B Wilks, D B Miracle, C P Chuang and P K Liaw, Refractory high-entropy alloys, *Intermetallics* **18** 1758 (2010). doi:10.1016/j.intermet.2010.05.014

6 O N Senkov, D B Miracle, K J Chaput and J-P Couzinie, Development and exploration of refractory high entropy alloys—a review, *J. Mater. Res.* **33** 3092 (2018). doi:10.1557/jmr.2018.153

7 D B Miracle and O N Senkov, A critical review of high entropy alloys and related concepts, *Acta Mater.* **122** 448 (2017). doi:10.1016/j.actamat.2016.08.081

8 E P George, D Raabe and R O Ritchie, High-entropy alloys, *Nat. Rev. Mater.* **4** 515 (2019). doi:10.1038/s41578-019-0121-4

9 Y Zhang *et al*, Microstructures and properties of high-entropy alloys, *Prog. Mater. Sci.* **61** 1 (2014). doi:10.1016/j.pmatsci.2013.10.001

10 M C Troparevsky, J R Morris, P R C Kent, A R Lupini and G M Stocks, Criteria for predicting the formation of single-phase high-entropy alloys, *Phys. Rev. X* **5** 011041 (2015). doi:10.1103/PhysRevX.5.011041

11 F Otto, Y Yang, H Bei and E P George, Relative effects of enthalpy and entropy on the phase stability of equiatomic high-entropy alloys, *Acta Mater.* **61** 2628 (2013). doi:10.1016/j.actamat.2013.01.042

12 X Yang and Y Zhang, Prediction of high-entropy stabilized solid-solution in multi-component alloys, *Mater. Chem. Phys.* **132** 233 (2012). doi:10.1016/j.matchemphys.2011.11.021

13 O El-Atwani *et al*, Outstanding radiation resistance of tungsten-based high-entropy alloys, *Sci. Adv.* **5** eaav2002 (2019). doi:10.1126/sciadv.aav2002

14 A Zunger, S-H Wei, L G Ferreira and J E Bernard, Special quasirandom structures, *Phys. Rev. Lett.* **65** 353 (1990). doi:10.1103/PhysRevLett.65.353

15 A van de Walle *et al*, Efficient stochastic generation of special quasirandom structures, *Calphad* **42** 13 (2013). doi:10.1016/j.calphad.2013.06.006

16 P Giannozzi *et al*, QUANTUM ESPRESSO: a modular and open-source software project for quantum simulations of materials, *J. Phys.: Condens. Matter* **21** 395502 (2009). doi:10.1088/0953-8984/21/39/395502

17 P Giannozzi *et al*, Advanced capabilities for materials modelling with Quantum ESPRESSO, *J. Phys.: Condens. Matter* **29** 465901 (2017). doi:10.1088/1361-648X/aa8f79

18 P Giannozzi *et al*, Quantum ESPRESSO toward the exascale, *J. Chem. Phys.* **152** 154105 (2020). doi:10.1063/5.0005082

19 J P Perdew, K Burke and M Ernzerhof, Generalized gradient approximation made simple, *Phys. Rev. Lett.* **77** 3865 (1996). doi:10.1103/PhysRevLett.77.3865

20 P E Bl\"ochl, Projector augmented-wave method, *Phys. Rev. B* **50** 17953 (1994). doi:10.1103/PhysRevB.50.17953

21 G Kresse and D Joubert, From ultrasoft pseudopotentials to the projector augmented-wave method, *Phys. Rev. B* **59** 1758 (1999). doi:10.1103/PhysRevB.59.1758

22 H J Monkhorst and J D Pack, Special points for Brillouin-zone integrations, *Phys. Rev. B* **13** 5188 (1976). doi:10.1103/PhysRevB.13.5188

COLOPHON

How this document was made

The Kronos Fleet — Combined Editorial, 2026 is set in **Fraunces** (display), **Gelasio** (text), and **IBM Plex Mono** (data & equations), carried forward from the Kronos editorial design system.

The figures are rendered at 300 dpi from the deposited generator scripts; the document is composed as a single self-contained file with embedded fonts and imagery, paginated to US Letter, and rendered to PDF through a headless Chromium engine in matched light and dark editions.

Every headline quantity carries an evidence class; withdrawn and restated values are marked as such. Nothing herein is frozen beyond the founder-approved Tier-A set.

Explore it live — turn the interactive 3-D model, run the deposited solvers in the physics validator, and watch the companion film series.

◆

LEGAL NOTICE

Notice, status, and distribution

Conceptual design & simulation study. This document reports a conceptual design and simulation study. It is not a construction commitment, a safety-analysis report, a regulatory filing, or an offer of securities. Forward-looking statements — schedules, costs, market sizes, and performance — are estimates subject to the limitations set out in the Simulations part and may change.

Numbers and their classes. Quantities are reported with evidence classes and case labels; modelled, assumed, and requirement-class values are identified as such and are not to be quoted without their labels.

Public edition. This edition carries the physics and design only; all financial, funding, and defense-commercial content has been removed for public distribution. The scientific text corresponds to the arXiv and journal submissions.

THE 2026 KRONOS SERIES

One programme, many papers

This editorial is one paper in the Kronos 2026 series — a real fusion company's complete, reproducible physics record for a spherical-tokamak breeder and its low-neutron D–^{3}He tandem-mirror burners. Every headline number is a frozen anchor in the Physics De-Risking Register.

Explore the whole programme: the De-Risking Register, the interactive 3-D model, and the physics validator.

KRONOS FUSION ENERGY

A Tantalum- and Rhenium-Free Low-Activation Alloy Family for First Wall, Divertor and Direct-Energy-Converter Electrodes: A First-Principles Composition-of-Matter Study

A real fusion company building real machines. Explore the science, live.

Zenodo · doi:10.5281/zenodo.22645891

Read on kronosfusionenergy.com

The Physics De-Risking Register